Deep Learning-assisted Automatic Modulation Classification using Spectrograms

Hamza Ouamna
Laboratory of Advanced Systems Engineering (ISA), Electrical Telecommunications Department, National School of Applied Sciences (ENSA), Ibn Tofail University, Kenitra, Morocco
hamza.ouamna@uit.ac.ma (corresponding author)

Anass Kharbouche
Laboratory of Advanced Systems Engineering (ISA), Electrical Telecommunications Department, National School of Applied Sciences (ENSA), Ibn Tofail University, Kenitra, Morocco
anass.kharbouche@uit.ac.ma

Zhour Madini
Laboratory of Advanced Systems Engineering (ISA), Electrical Telecommunications Department, National School of Applied Sciences (ENSA), Ibn Tofail University, Kenitra, Morocco
zhour.madini@uit.ac.ma

Younes Zouine
Laboratory of Advanced Systems Engineering (ISA), Electrical Telecommunications Department, National School of Applied Sciences (ENSA), Ibn Tofail University, Kenitra, Morocco
younes.zouine@uit.ac.ma

Received: 19 October 2024 | Revised: 25 November 2024 and 8 December 2024 | Accepted: 12 December 2024

 DOI: https://doi.org/10.48084/etasr.9334

ABSTRACT

With the increasing demand for reliable and efficient V2X (Vehicle-to-Everything) communications in cognitive radio environments, spectrum sharing becomes imperative. In this context, accurate modulation classification serves as a fundamental component for efficient spectrum sensing and allocation. This paper proposes a novel approach utilizing Convolutional Neural Networks (CNNs) trained on spectrograms of BPSK and QPSK modulation schemes for automatic modulation classification in V2X scenarios. Experimental results demonstrated the effectiveness of the proposed CNN-based framework in accurately classifying modulation schemes in V2X communications.

Keywords-automatic modulation classification; cognitive radio; BPSK; QPSK; CNN; Alexnet; V2X

I. INTRODUCTION

The rise of cognitive radio and connected cars has created a need for reliable and efficient wireless communication systems. One key challenge in these systems is Automatic Modulation Classification (AMC), which involves identifying the modulation scheme used to transmit signals over a wireless channel. Traditional approaches to AMC have limitations, particularly in dealing with varying channel conditions and multiple modulation schemes [1, 2]. Deep Learning (DL) [3] has shown promising results in improving AMC performance, particularly in the presence of channel impairments. DL is a subset of machine learning that involves training artificial neural networks to learn and make predictions on complex data [4, 5]. DL models can effectively learn the underlying characteristics of radio signals for modulation pattern recognition, leading to improved classification performance [6, 7]. In cognitive radio systems, where the available spectrum is dynamically allocated based on real-time demand, DL-based AMC can improve spectrum utilization [8, 9] and reduce interference. Similarly, in connected cars, where reliable communication is critical to safety and performance, DL-based AMC can improve signal quality and reduce latency. Recent research has explored DL-based AMC approaches in both cognitive radio and connected cars with promising results. Recent studies have proposed DL-based AMC methods using Convolutional Neural Networks (CNNs) to classify signals in cognitive radio networks with dynamic spectrum access. Other studies have proposed DL-based AMC methods using a hybrid CNN-Recurrent Neural Network (RNN) approach for connected cars [10, 11]. Overall, DL-based AMC has the potential to improve wireless communication systems in

cognitive radio and connected car applications, leading to more reliable and efficient performance.

II. MATERIALS AND METHODS

This section presents the proposed AMC system design. To evaluate the proposed system, RadioML 2016.10A was used, which is an RF dataset for machine learning developed by Deepsig Inc. [12].

A. System Model

The system begins with preprocessing of raw signal data, adapting it into a suitable format for CNN-based analysis. The neural network is designed to capture and understand intricate modulation patterns. The training process involves optimizing the network's parameters [13]. The proposed system model was evaluated using standard metrics [14, 15].

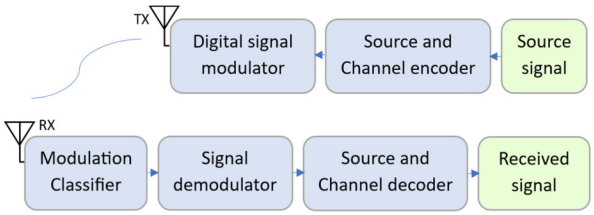

Fig. 1. Digital communication model.

B. Mathematical Model

This section describes the mathematical modeling of IQ data using BPSK and QPSK modulation schemes, as well as the noise characteristics of the RadioML 2016.10A dataset. The representation of complex baseband signals, noise modeling, and the impact of Signal-to-Noise Ratio (SNR) are discussed in detail.

1) Complex Baseband Signal Representation

In a digital communication system, the transmitted signal is represented using In-phase (I) and Quadrature (Q) components, which form the complex baseband signal. Mathematically, this signal can be expressed as:

$$s(t) = I(t) + jQ(t) \quad (1)$$

where $s(t)$ is the complex baseband signal, $I(t)$ is the in-phase component of the signal, and $Q(t)$ is the quadrature-phase component of the signal.

2) Binary Phase Shift Keying (BPSK)

In BPSK, each symbol represents a single bit, resulting in two possible phase states: 0 and π. The transmitted BPSK signal can be represented as:

$$s(t) = Acos(2\pi f_c t + \pi m) \quad (2)$$

where A is the amplitude of the signal, f_c is the carrier frequency, and $m \in \{0,1\}$ is the bit being transmitted. In complex form, the BPSK signal is expressed as:

$$s[n] = A * (1 - 2m) = \pm A \quad (3)$$

where A is a constant amplitude and m is the binary symbol (0 or 1), mapped to either $+A$ or $-A$. This representation simplifies to a purely real signal with $Q = 0$, meaning the modulation only affects the in-phase component.

3) Quadrature Phase Shift Keying (QPSK)

In QPSK, each symbol represents 2 bits, allowing four possible phase shifts: 0, $\frac{\pi}{2}$, π and $\frac{3\pi}{2}$. The QPSK signal is represented as:

$$s(t) = Acos(2\pi f_c t + \theta_i) + jAsin(2\pi f_c t + \theta_i) \quad (4)$$

where A is the signal amplitude and $\theta_i \in \{0, \frac{\pi}{2}, \pi, \frac{3\pi}{2}\}$ represents the phase corresponding to the transmitted symbol. The complex representation for QPSK is given by:

$$s[n] = A(I[n] + jQ[n]) \quad (5)$$

where $I[n], Q[n] \in \{\pm 1\}$ represent the in-phase and quadrature components. Each 2-bit pair is mapped to a unique phase shift, such as:

- $00 \rightarrow A + jA$
- $01 \rightarrow -A + jA$
- $10 \rightarrow A - jA$
- $11 \rightarrow -A - jA$

This mapping enables QPSK to achieve higher data rates compared to BPSK by encoding more bits per symbol.

4) Noise Model

In real-world communication systems, signals are subject to noise, which affects their integrity. The RadioML 2016.10A dataset introduces noise in the form of Additive White Gaussian Noise (AWGN) to simulate different SNRs. The received signal is thus modeled as:

$$r[n] = s[n] + w[n] \quad (6)$$

where $r[n]$ is the received noisy signal, $s[n]$ is the transmitted modulated signal, and $w[n]$ is the noise component, modeled as a complex Gaussian random variable. The noise $w[n]$ is decomposed into its in-phase and quadrature components:

$$w[n] = w_I[n] + jw_Q[n] \quad (7)$$

where $w_I[n]$ is the noise affecting the in-phase component $I(t)$ and $w_Q[n]$ is the noise affecting the quadrature component $Q(t)$.

Both $w_I[n]$ and $w_Q[n]$ are drawn from a Gaussian distribution with mean zero and variance σ^2. The noise components are independent and identically distributed.

5) Signal-to-Noise Ratio (SNR)

SNR is a key metric that quantifies the relative power of the signal compared to the noise power. It is defined as:

$$SNR = \frac{P_s}{P_w} \quad (8)$$

where P_s is the average power of the transmitted signal $s[n]$, and P_w is the average power of the noise $w[n]$. In discrete form, the SNR is given by:

$$SNR = \frac{\mathbb{E}[|s[n]|^2]}{\mathbb{E}[|w[n]|^2]} \quad (9)$$

The RadioML 2016.10A dataset includes data at various SNR levels, ranging from -20 to 18 dB, to simulate different channel conditions. As the SNR decreases, the impact of noise becomes more significant, making it challenging for a classifier to distinguish between different modulation types.

6) Received Signal Representation

After adding noise, the received signals for BPSK and QPSK can be written as in (10) and (11), respectively.

$$r[n] = \pm A + w_I[n] \quad (10)$$

In this case, the noise is added directly to the in-phase component of the signal.

$$r[n] = (I[n] + w_I[n]) + j(Q[n] + w_Q[n]) \quad (11)$$

For QPSK, noise affects both the in-phase and quadrature-phase components equally [16, 17].

C. Proposed Architecture

Figure 2 shows the proposed feature image-based AMC architecture. The AMC part consists of a feature extractor and a CNN classifier. When the AMC scheme has received the signals, the feature extractor extracts the features and transforms them into an image. Then, CNN classifies the modulation type based on previous learning [18].

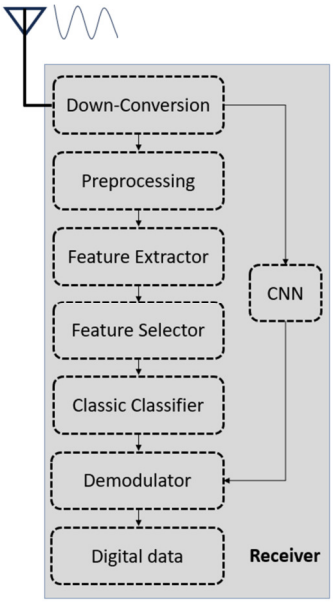

Fig. 2. CNN-based AMC architecture.

Initially, the dataset is divided into training and testing sets with an 80:20 split. Preprocessing steps convert the raw signal data into spectrograms. These spectrograms are then normalized to a consistent range, typically between 0 and 1, to facilitate stable model training. Following normalization, the spectrogram images are reshaped to a uniform dimension, ensuring consistency in input size and format for the neural network.

Once preprocessing is complete, the training phase involves feeding the augmented spectrograms into the neural network, where the model learns to classify BPSK and QPSK signals through backpropagation and optimization algorithms. During training, the model's performance is monitored to prevent overfitting using methods such as early stopping and dropout [19, 20].

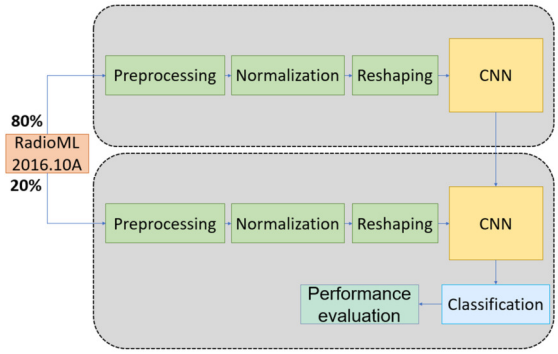

Fig. 3. Methodology.

III. SIMULATIONS AND DISCUSSION

A. Description of Experimental Dataset

The RadioML 2016.10A dataset was used to evaluate the performance of the proposed model, which comprises 220,000 samples with 11 different modulation types. The dataset was generated using a software-defined radio to perform I/Q dual-channel sampling, with a data length of 128. The SNR of the samples ranges from -20 dB to 18 dB, with a step size of 2 dB. The channel noise is white Gaussian noise. The dataset includes various modulation types, such as BPSK, QPSK, 8PSK, AM-DSB, AM-SSB, CPFSK, GFSK, PAM4, QAM16, QAM64, and WBFM. The sampling frequency is set at 200 KHz, with a sample length of 128. The dataset includes sampling rate and carrier frequency offsets with standard deviations of 0.01 Hz and maximum offsets of 50 and 500 Hz, respectively. Table I summarizes dataset parameters and components [21, 22].

TABLE I. DATASET PARAMETERS AND COMPONENTS

RadioML 2016.10A	
Parameter	**Value**
Sampling frequency	200 KHz
Sampling rate offset standard deviation	0.01 Hz
Maximum sampling rate offset	50 Hz
Carrier frequency offset standard deviation	0.01 Hz
Maximum carrier frequency offset	500 Hz
Sample length	128
SNR range	-20 to 18 dB
Modulations	8PSK, AM-DSB, AM-SSB, BPSK, CPFSK, GFSK, PAM4, QAM16, QAM64, QPSK, WBFM

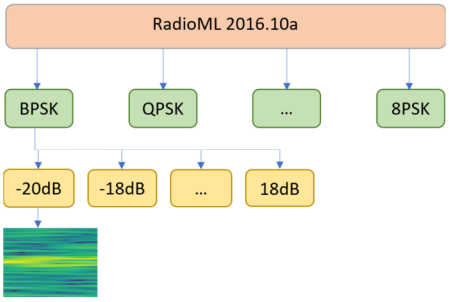

Fig. 4. DeepSig Inc. RadioML 2016.10A dataset structure.

Figure 5 illustrates BPSK and QPSK signals at various SNR levels (-20, 0, and 18 dB). These spectrograms visually demonstrate how signal clarity improves with higher SNR, providing a critical link between the dataset's quantitative parameters and their practical impact on signal quality.

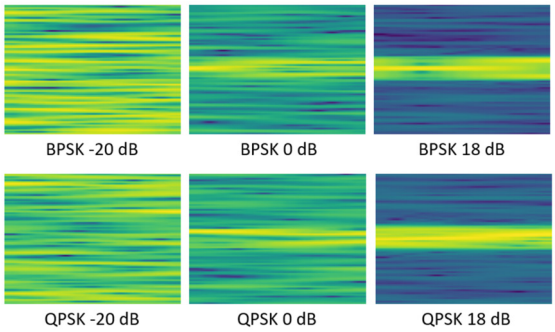

Fig. 5. BPSK and QPSK spectrograms for different SNRs.

B. Proposed Models

CNNs are particularly influential in image processing due to their unique architecture. In contrast to traditional fully connected networks, CNNs exhibit distinctive characteristics that contribute to their efficacy. Local connection entails that each neuron is connected to only a small subset of neurons in the preceding layer, significantly reducing the number of parameters. Weight sharing allows a set of connections to share the same weight, eliminating the need for individual weights for each connection and further reducing parameters. Lastly, downsampling, achieved through the pooling layer, decreases the number of samples per layer, diminishing parameters while concurrently enhancing model robustness [23, 24].

1) AMC-CNN Model

The architecture, presented in Figure 6, starts with three convolutional layers, each characterized by a Rectified Linear Unit (ReLU) activation function, and the network progressively reduces spatial dimensions through MaxPooling layers. The flattened output is fed into fully connected layers with 128 and 64 neurons, each employing ReLU activation functions, culminating in an output layer with 2 neurons and a Softmax activation function suitable for multiclass classification tasks. The model is compiled using the Adam optimizer and categorical cross-entropy loss [25]. The training was performed with a batch size of 100 over 100 epochs and a validation split of 20%.

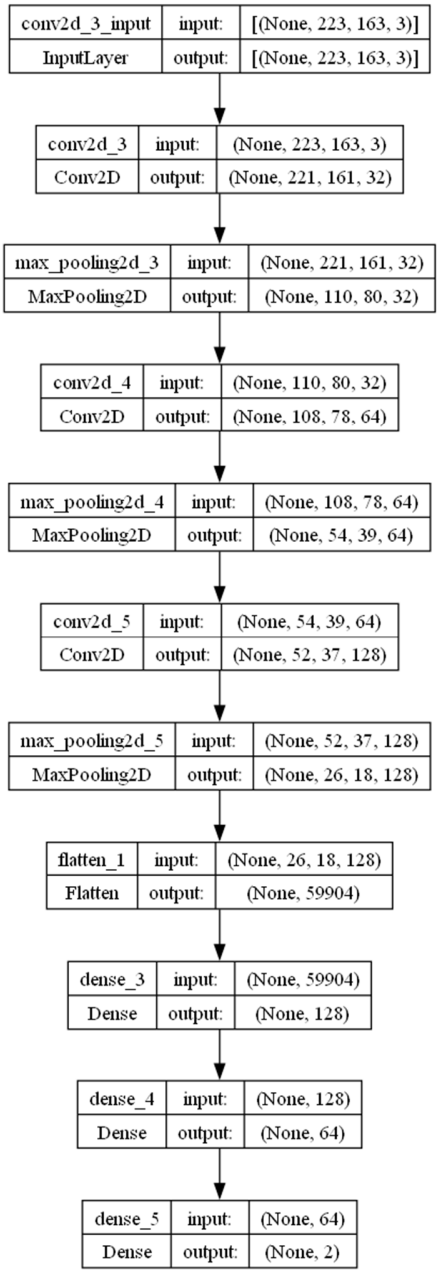

Fig. 6. AMC-CNN implementation.

2) AMC-AlexNet Model

AlexNet is a CNN, presented in Figure 7, that is 8 layers deep, featuring convolutional layers with varying filter sizes and max-pooling for spatial reduction, followed by a flattening step. Subsequently, three fully connected layers are integrated with decreasing neuron counts. The output layer, designed for multiclass classification, consists of 2 neurons utilizing a softmax activation function. The model is trained using the Adam optimizer and categorical cross-entropy loss, with the training history tracked over 100 epochs and a batch size of 100, including a validation split of 20% [26, 27].

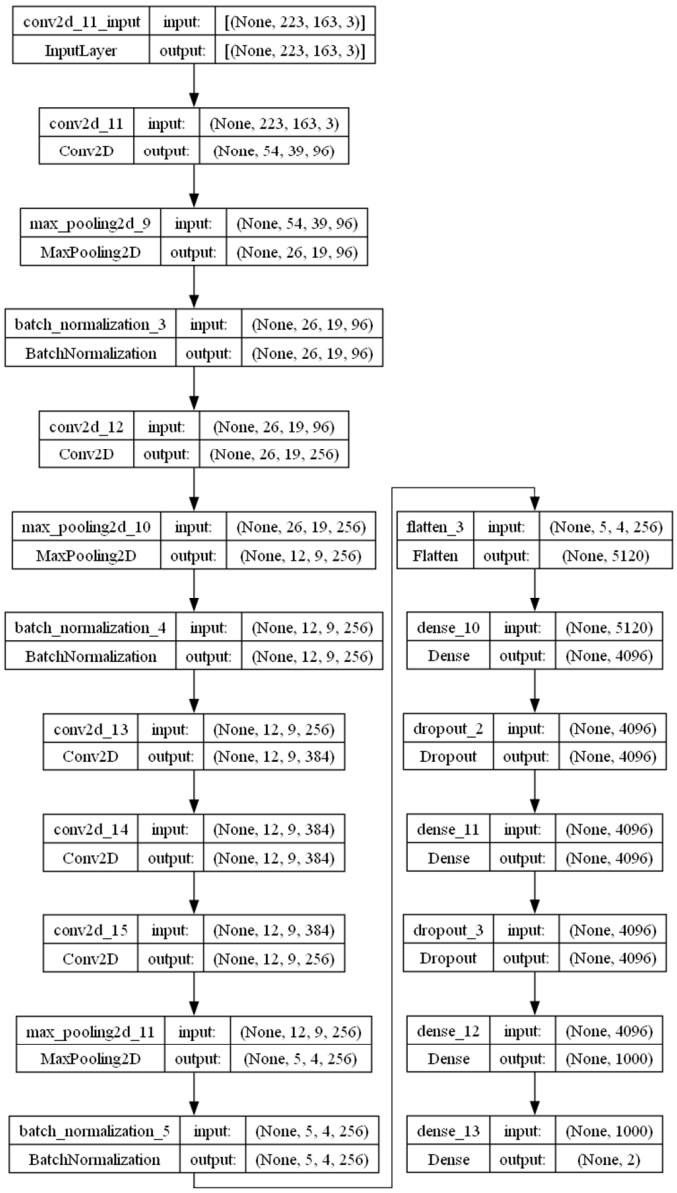

Fig. 7. AMC-Alexnet implementation.

C. Experimental procedure

1) Categorical Cross-Entropy

Categorical cross-entropy [24] is a commonly used loss function in multiclass classification problems. It measures the difference between the true distribution (labels) and the predicted distribution (model outputs). For a single instance, the categorical cross-entropy loss is defined as:

$$L = -\sum_{i=1}^{N} y_i \log(p_i) \quad (4)$$

where N is the number of classes, y_i is the binary indicator (0 or 1) if class label i is the correct classification, and p_i is the predicted probability of class i. In practice, categorical cross-entropy is used to train models to produce probabilities that closely match the true class distributions, minimizing the loss to improve classification accuracy.

2) Hyperparameters

Hyperparameters included learning rate, batch size, number of epochs, and the choice of optimizer and loss function. Table II summarizes these critical hyperparameters, providing a foundation for effective model development and tuning.

TABLE II. HYPERPARAMETERS

Hyperparameters		
Parameter	**CNN**	**Alexnet**
Optimizer	Adam	Adam
Epochs	100	100
Batch size	100	100
Loss function	Categorical cross-entropy	Categorical cross-entropy
Learning rate	0.001	0.001
Total parameters	7769474 (29.64 MB)	45605562 (173.97 MB)
Trainable parameters	7769474 (29.64 MB)	45604346 (173.97 MB)
Non-trainable parameters	0 (0.00 Byte)	1216 (4.75 KB)

3) AMC-CNN Training Results

The CNN classifier demonstrated substantial improvement over 100 epochs. The training loss decreased from 0.6978 to 0.0001, while the accuracy increased from 52.65% to 100%. The validation loss started at 0.6627 and reached 3.4710, with the validation accuracy increasing from 58.92% to 75.50%. These results indicate the model's strong learning capability and effective training progression. The final training accuracy of 100% suggests that the model effectively captured the signal characteristics. The validation accuracy stabilizing at 75.50% reflects consistent performance on unseen data.

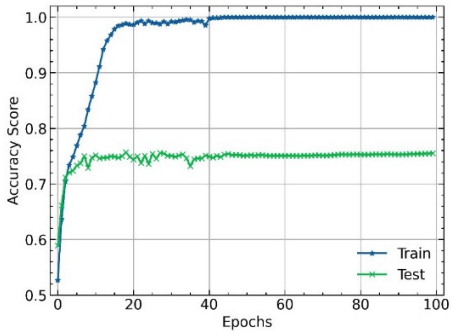

Fig. 8. Model accuracy.

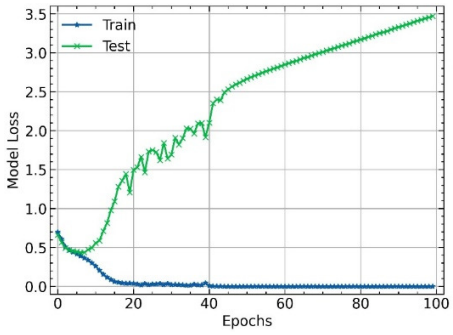

Fig. 9. Model loss.

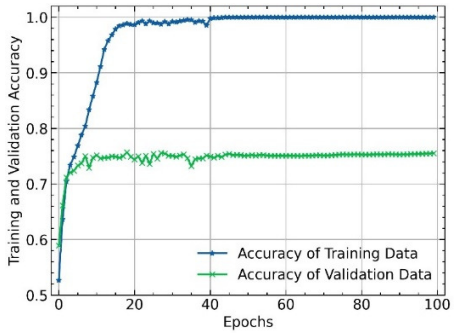

Fig. 10. Training and validation accuracy.

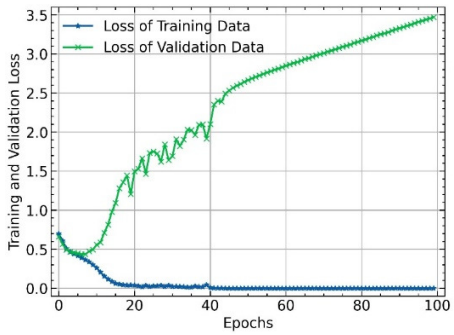

Fig. 11. Training and validation loss.

4) AMC-Alexnet Training Results

The training and validation performance of the model over 100 epochs showed significant improvement. Training loss was reduced from 1.85 to 0.31, and training accuracy increased from 28.44% to 84.97%. The validation loss initially fluctuated, peaking at 3.73, and eventually stabilized at 3.07. Meanwhile, the validation accuracy improved from 29.19% to 43.48%. These results indicate effective learning in training.

D. Model Testing

This study systematically assessed the performance of the proposed model across a diverse range of SNRs, spanning from -20 to 18 dB. This testing method aimed to evaluate the robustness of the model in the presence of varying levels of noise. By examining key metrics such as accuracy across this broad range, valuable insights can be gained into the network's ability to handle both low and high SNR scenarios.

E. Analysis of Results

1) Performance Metrics

The performance of modulation classification is usually measured by the accuracy metric, which can be generally calculated as follows:

$$Accuracy = \frac{TP+TN}{TP+TN+FP+FN} \quad (5)$$

where *TP*, *TN*, *FP*, and *FN* denote True Positives, True Negatives, False Positives, and False Negatives, respectively. The results can be reported using confusion matrices, which are commonly used in the machine learning domain [28, 29].

2) SNR Range Effect in Test Results

The SNR is critical in AMC, as it affects the classification accuracy, and low SNRs challenge the discrimination of similar modulations. Testing across SNR levels ensures model robustness in real-world conditions. It also enables fair benchmarking and highlights areas for optimization in noisy environments. Proper SNR selection ensures reliable performance evaluation [30, 31].

Choosing an SNR range from -20 to 18 dB is vital, as it covers extreme noise conditions to near-ideal scenarios. Low SNRs (e.g., -20 dB) test the model's ability to classify under heavy noise, while higher SNRs (e.g., 18 dB) evaluate performance with clearer signals.

3) AMC-CNN Testing Results

The confusion matrix, shown in Figure 12, reveals that the CNN accurately classified 1584 BPSK and 1467 QPSK signals while misclassifying 436 BPSK as QPSK and 506 QPSK as BPSK. This indicates a high classification accuracy but also highlights the presence of some misclassification errors between the two signal types. The Probability Of Detection (POD) generally increases as the SNR improves. At lower SNR values, the POD fluctuated but started to consistently increase above 50% as SNR reached -4 dB. The CNN achieved over 90% POD at 0 dB and maintained high accuracy (95-98%) for SNR values above 10 dB.

4) AMC-Alexnet Testing Results

The AlexNet model demonstrated similar performance. Both models exhibited proficiency in signal classification with minor differences in misclassification rates. The transfer learning application of AlexNet for BPSK and QPSK signal classification shows a POD increase with increasing SNR. Initially fluctuating around 50% at low SNR values, it improved considerably from -6 dB onward. Exceeding 90% at 0 dB and 98% at 2 dB, it maintained robust accuracy (95-99%) for SNRs above 10 dB.

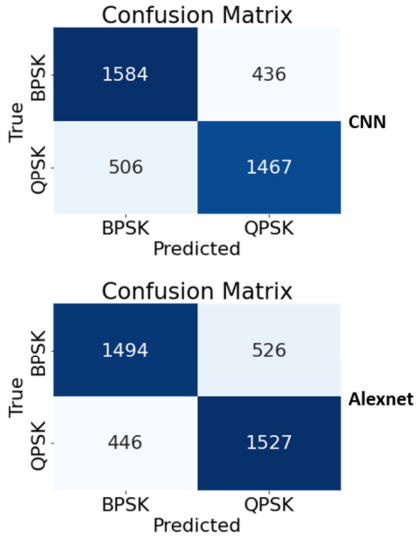

Fig. 12. Confusion matrices.

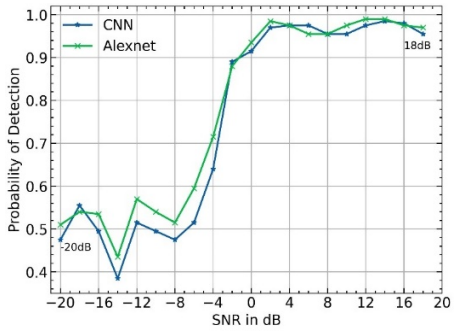

Fig. 13. Probability Of Detection (POD) vs. SNR.

5) Performance Metrics Comparison with Prior Works

Table III provides a performance comparison of different automatic modulation recognition methods.

TABLE III. PERFORMANCE METRICS COMPARISON

Ref.	Model	Modulations	Results
[32]	4-layer CNN	11	80% at 0 dB <60% at -5 dB
[33]	CNNs : AlexNet VGG16 VGG19 Resnet18	07	At 5 dB: 82% 86% 87% 91%
[34]	BiLSTM	06 Radar Waveforms	83% at 0 dB
Proposed	CNN	2	97.5 % at 6 dB 91.5% at 0 dB 64% at -4 dB
Proposed	Alexnet	2	95.5 % at 6 dB 93.5% at 0 dB 71.5% at -4 dB

These results clearly demonstrate that advanced models, such as CNN-based architectures, achieve higher accuracy compared to traditional methods such as BiLSTM, especially at challenging SNR levels. The CNN-based model achieved 97.5% accuracy at 6 dB, 91.5% at 0 dB, and maintained competitive results at -4 dB, showcasing robustness even in low-SNR scenarios. Similarly, the AlexNet-based model showed strong results.

IV. CONCLUSION

The proposed models demonstrated superior performance in AMC, significantly outperforming existing approaches under various SNR conditions. A key contribution of this research is the targeted training approach, which focuses on resolving confusion between closely spaced modulations, such as BPSK and QPSK, that share similar spectral properties. Addressing these challenging classes enhances the model's ability to differentiate between them, leading to improved overall classification accuracy. Future work will explore broader modulation schemes and real-world datasets to further refine the models, ensuring their practical applicability in dynamic spectrum access scenarios, particularly for V2X communications, where reliable data transmission is crucial in challenging wireless environments. Additionally, integrating these models into a Multi-Task Learning (MTL) framework could further enhance their ability to distinguish between confusing modulation classes, improving overall performance.

ACKNOWLEDGMENT

The authors declare no competing financial interests or personal relationships that could have appeared to influence the work reported in this paper.

REFERENCES

[1] N. El-Haryqy, Z. Madini, Y. Zouine, and A. Kharbouche, "A Survey on Automatic Signal Detection Using Deep Learning," in *2023 9th International Conference on Optimization and Applications (ICOA)*, AbuDhabi, United Arab Emirates, Oct. 2023, pp. 1–6, https://doi.org/10.1109/ICOA58279.2023.10308833.

[2] K. Kimani and M. Njiraine, "Cognitive Radio Spectrum Sensing Mechanisms in TV White Spaces: A Survey," *Engineering, Technology & Applied Science Research*, vol. 8, no. 6, pp. 3673–3680, Dec. 2018, https://doi.org/10.48084/etasr.2442.

[3] A. Kharbouche, Z. Madini, and Y. Zouine, "Performance improvements of a VLC system, in a V2X context, using a different multiplexing technique," *TELKOMNIKA (Telecommunication Computing Electronics and Control)*, vol. 21, no. 4, pp. 725–735, Aug. 2023, https://doi.org/10.12928/telkomnika.v21i4.24042.

[4] A. Kharbouche, Z. Madini, Y. Zouine, and N. El-Haryqy, "Signal demodulation with Deep Learning Methods for visible light communication," in *2023 9th International Conference on Optimization and Applications (ICOA)*, AbuDhabi, United Arab Emirates, Oct. 2023, pp. 1–5, https://doi.org/10.1109/ICOA58279.2023.10308822.

[5] H. Shahinzadeh, A. Mahmoudi, A. Asilian, H. Sadrarhami, M. Hemmati, and Y. Saberi, "Deep Learning: A Overview of Theory and Architectures," in *2024 20th CSI International Symposium on Artificial Intelligence and Signal Processing (AISP)*, Babol, Iran, Feb. 2024, pp. 1–11, https://doi.org/10.1109/AISP61396.2024.10475265.

[6] H. Huang, J. Yang, H. Huang, Y. Song, and G. Gui, "Deep Learning for Super-Resolution Channel Estimation and DOA Estimation Based Massive MIMO System," *IEEE Transactions on Vehicular Technology*, vol. 67, no. 9, pp. 8549–8560, Sep. 2018, https://doi.org/10.1109/TVT.2018.2851783.

[7] X. Zhao, X. Li, and Z. Zhang, "Joint Structural Learning to Rank with Deep Linear Feature Learning," *IEEE Transactions on Knowledge and Data Engineering*, vol. 27, no. 10, pp. 2756–2769, Jul. 2015, https://doi.org/10.1109/TKDE.2015.2426707.

[8] Y. Li, X. Cheng, and G. Gui, "Co-Robust-ADMM-Net: Joint ADMM Framework and DNN for Robust Sparse Composite Regularization," *IEEE Access*, vol. 6, pp. 47943–47952, 2018, https://doi.org/10.1109/ACCESS.2018.2867435.

[9] C. S. Park, J. H. Choi, S. P. Nah, W. Jang, and D. Y. Kim, "Automatic Modulation Recognition of Digital Signals using Wavelet Features and SVM," in *2008 10th International Conference on Advanced Communication Technology*, Gangwon-Do, South Korea, Feb. 2008, pp. 387–390, https://doi.org/10.1109/ICACT.2008.4493784.

[10] Z. Md. Fadlullah, F. Tang, B. Mao, J. Liu, and N. Kato, "On Intelligent Traffic Control for Large-Scale Heterogeneous Networks: A Value Matrix-Based Deep Learning Approach," *IEEE Communications Letters*, vol. 22, no. 12, pp. 2479–2482, Sep. 2018, https://doi.org/10.1109/LCOMM.2018.2875431.

[11] F. Tang *et al.*, "On Removing Routing Protocol from Future Wireless Networks: A Real-time Deep Learning Approach for Intelligent Traffic Control," *IEEE Wireless Communications*, vol. 25, no. 1, pp. 154–160, Feb. 2018, https://doi.org/10.1109/MWC.2017.1700244.

[12] T. J. O'Shea and N. West, "Radio Machine Learning Dataset Generation with GNU Radio," *Proceedings of the GNU Radio Conference*, vol. 1, no. 1, Sep. 2016.

[13] F. Meng, P. Chen, L. Wu, and X. Wang, "Automatic Modulation Classification: A Deep Learning Enabled Approach," *IEEE Transactions on Vehicular Technology*, vol. 67, no. 11, pp. 10760–10772, Aug. 2018, https://doi.org/10.1109/TVT.2018.2868698.

[14] W. Xie, S. Hu, C. Yu, P. Zhu, X. Peng, and J. Ouyang, "Deep Learning in Digital Modulation Recognition Using High Order Cumulants," *IEEE Access*, vol. 7, pp. 63760–63766, 2019, https://doi.org/10.1109/ACCESS.2019.2916833.

[15] Y. Wang, M. Liu, J. Yang, and G. Gui, "Data-Driven Deep Learning for Automatic Modulation Recognition in Cognitive Radios," *IEEE Transactions on Vehicular Technology*, vol. 68, no. 4, pp. 4074–4077, Apr. 2019, https://doi.org/10.1109/TVT.2019.2900460.

[16] M. W. Aslam, Z. Zhu, and A. K. Nandi, "Automatic Modulation Classification Using Combination of Genetic Programming and KNN," *IEEE Transactions on Wireless Communications*, vol. 11, no. 8, pp. 2742–2750, Aug. 2012, https://doi.org/10.1109/TWC.2012.060412.110460.

[17] V. S. Doan, T. Huynh-The, C. H. Hua, Q. V. Pham, and D. S. Kim, "Learning Constellation Map with Deep CNN for Accurate Modulation Recognition," in *GLOBECOM 2020 - 2020 IEEE Global Communications Conference*, Taipei, Taiwan, Dec. 2020, pp. 1–6, https://doi.org/10.1109/GLOBECOM42002.2020.9348129.

[18] T. J. O'Shea, T. Roy, and T. C. Clancy, "Over-the-Air Deep Learning Based Radio Signal Classification," *IEEE Journal of Selected Topics in Signal Processing*, vol. 12, no. 1, pp. 168–179, Oct. 2018, https://doi.org/10.1109/JSTSP.2018.2797022.

[19] S. Tridgell, D. Boland, P. H. W. Leong, R. Kastner, A. Khodamoradi, and Siddhartha, "Real-time Automatic Modulation Classification using RFSoC," in *2020 IEEE International Parallel and Distributed Processing Symposium Workshops (IPDPSW)*, New Orleans, LA, USA, May 2020, pp. 82–89, https://doi.org/10.1109/IPDPSW50202.2020.00021.

[20] J. Kaiser, H. Mostafa, and E. Neftci, "Synaptic Plasticity Dynamics for Deep Continuous Local Learning (DECOLLE)," *Frontiers in Neuroscience*, vol. 14, May 2020, https://doi.org/10.3389/fnins.2020.00424.

[21] A. Tsakmalis, S. Chatzinotas, and B. Ottersten, "Modulation and Coding Classification for Adaptive Power Control in 5G Cognitive Communications," in *2014 IEEE 15th International Workshop on Signal Processing Advances in Wireless Communications (SPAWC)*, Toronto, ON, Canada, Jun. 2014, pp. 234–238, https://doi.org/10.1109/SPAWC.2014.6941505.

[22] O. F. Abd-Elaziz, M. Abdalla, and R. A. Elsayed, "Deep Learning-Based Automatic Modulation Classification Using Robust CNN Architecture for Cognitive Radio Networks," *Sensors*, vol. 23, no. 23, Jan. 2023, Art. no. 9467, https://doi.org/10.3390/s23239467.

[23] F. Wang, T. Shang, C. Hu, and Q. Liu, "Automatic Modulation Classification Using Hybrid Data Augmentation and Lightweight Neural Network," *Sensors*, vol. 23, no. 9, Jan. 2023, Art. no. 4187, https://doi.org/10.3390/s23094187.

[24] K. P. Murphy, Machine Learning: A Probabilistic Perspective. MIT Press, 2012.

[25] J. A. Snoap, D. C. Popescu, J. A. Latshaw, and C. M. Spooner, "Deep-Learning-Based Classification of Digitally Modulated Signals Using Capsule Networks and Cyclic Cumulants," *Sensors*, vol. 23, no. 12, Jan. 2023, Art. no. 5735, https://doi.org/10.3390/s23125735.

[26] A. Kumar, S. Majhi, G. Gui, H. C. Wu, and C. Yuen, "A Survey of Blind Modulation Classification Techniques for OFDM Signals," *Sensors*, vol. 22, no. 3, Jan. 2022, Art. no. 1020, https://doi.org/10.3390/s22031020.

[27] S. Peng, H. Jiang, H. Wang, H. Alwageed, and Y.-D. Yao, "Modulation classification using convolutional Neural Network based deep learning model," in *2017 26th Wireless and Optical Communication Conference (WOCC)*, Newark, NJ, USA, Apr. 2017, pp. 1–5, https://doi.org/10.1109/WOCC.2017.7929000.

[28] P. Dileep, D. Das, and P. K. Bora, "Dense Layer Dropout Based CNN Architecture for Automatic Modulation Classification," in *2020 National Conference on Communications (NCC)*, Kharagpur, India, Feb. 2020, pp. 1–5, https://doi.org/10.1109/NCC48643.2020.9055989.

[29] T. Wang, G. Yang, P. Chen, Z. Xu, M. Jiang, and Q. Ye, "A Survey of Applications of Deep Learning in Radio Signal Modulation Recognition," *Applied Sciences*, vol. 12, no. 23, Jan. 2022, Art. no. 12052, https://doi.org/10.3390/app122312052.

[30] V. Pallam, H. Khan, S. R. Surampudi, and G. Immadi, "Reduced Kernel PCA Model for Nonlinear Spectrum Sensing in Cognitive Radio Network," *Journal of The Institution of Engineers (India): Series B*, Jun. 2024, https://doi.org/10.1007/s40031-024-01089-w.

[31] P. Venkatapathi, H. Khan, S. S. Rao, and G. Immadi, "Cooperative Spectrum Sensing Performance Assessment using Machine Learning in Cognitive Radio Sensor Networks," *Engineering, Technology & Applied Science Research*, vol. 14, no. 1, pp. 12875–12879, Feb. 2024, https://doi.org/10.48084/etasr.6639.

[32] Y. Zeng, M. Zhang, F. Han, Y. Gong, and J. Zhang, "Spectrum Analysis and Convolutional Neural Network for Automatic Modulation Recognition," *IEEE Wireless Communications Letters*, vol. 8, no. 3, pp. 929–932, Jun. 2019, https://doi.org/10.1109/LWC.2019.2900247.

[33] R. Liu, Y. Guo, and S. Zhu, "Modulation Recognition Method of Complex Modulation Signal Based on Convolution Neural Network," in *2020 IEEE 9th Joint International Information Technology and Artificial Intelligence Conference (ITAIC)*, Chongqing, China, Dec. 2020, pp. 1179–1184, https://doi.org/10.1109/ITAIC49862.2020.9338875.

[34] S. G. Bhatti and A. I. Bhatti, "Radar Signals Intrapulse Modulation Recognition Using Phase-Based STFT and BiLSTM," *IEEE Access*, vol. 10, pp. 80184–80194, 2022, https://doi.org/10.1109/ACCESS.2022.3195273.